

Peculiar Extended X-ray Emission around the “Radio-Loud” Black Hole Candidate 1E1740.7-2942

Wei Cui^{1,2}, N.S. Schulz¹, F.K. Baganoff¹, M.W. Bautz¹, J.P. Doty¹, G.P. Garmire³, I.F. Mirabel^{4,5}, G.R. Ricker¹, L.F. Rodríguez⁶, and S.C. Taylor¹

ABSTRACT

We present the discovery of peculiar extended X-ray emission around 1E1740.7-2942, a black hole candidate that is known to produce prominent, persistent radio jets. The data was obtained with the High-Energy Transmission Grating Spectrometer (HETGS) aboard the *Chandra X-ray Observatory*. The zeroth-order image reveals an elongated feature about $3''$ in length that is roughly *perpendicular* to the radio lobes (or jets). The feature is roughly symmetric about the point source. It is spatially resolved in the long direction but not in the short direction.

The position of 1E1740.7-2942 was determined with a statistical accuracy of $\sim 0.06''$ in the right ascension and $\sim 0.04''$ in the declination, thanks to *Chandra's* unprecedented spatial resolution. It is about $0.6''$ from the radio position but the difference is well within the uncertainty in the absolute aspect solutions of the observation. The dispersed HETGS spectra of 1E1740.7-2942 show evidence for the presence of weak, narrow emission lines, although the statistics are quite limited. We discuss possible origins of the extended emission and the implications of the emission lines.

Subject headings: binaries: general — stars: individual (1E1740.7-2942) — X-ray: stars

1. Introduction

Discovered by the *Einstein* satellite (Hertz & Grindlay 1984), 1E1740.7-2942 appears as a persistent X-ray source in the sky, only about $50'$ away from the center of the Galaxy. It is in fact

¹Center for Space Research, Massachusetts Institute of Technology, Cambridge, MA 02139

²Department of Physics, Purdue University, West Lafayette, IN 47907

³Department of Astronomy and Astrophysics, Pennsylvania State University, University Park, PA 16802

⁴Service d'Astrophysique, Centre d'Etudes de Saclay, 91191 Gif-sur-Yvette, France

⁵Instituto de Astronomía y Física del Espacio, Argentina

⁶Instituto de Astronomía, UNAM, Apartado Postal 70-264, 04510 México, DF, Mexico

the brightest persistent source at high energies ($\gtrsim 30$ keV) within a few degrees of the Galactic center (e.g., Skinner et al. 1987; Sunyaev et al. 1991). At low energies ($\lesssim 3$ keV), however, the X-ray emission from the source is strongly attenuated by the intervening matter along the line of sight. The inferred hydrogen column density is around 10^{23} cm^{-2} (see Sheth et al. 1996, Churazov et al. 1996, and Sakano et al. 1999 for most recent measurements), which is unusually high even for sources physically located near the Galactic center. Additional absorption can be attributed to the material associated with a molecular cloud in which the source is likely embedded (Bally & Leventhal 1991; Mirabel et al. 1991; Phillips et al. 1995; Yan & Dalgarno 1997).

1E1740.7-2942 has a very hard X-ray spectrum (measured up to ~ 300 keV; e.g., Skinner et al. 1991; Cook et al. 1991; Kuznetsov et al. 1997), which is characteristic of black hole candidates (BHCs) such as Cyg X-1. The source also shows strong aperiodic and quasi-periodic X-ray variability (Smith et al. 1997; Lin et al. 2000), again similar to BHCs. The observed X-ray properties, therefore, make 1E1740.7-2942 a BHC, although dynamical evidence for such a candidacy is still lacking. The high foreground extinction precludes the identification of the optical counterpart. Extensive searches for the infrared counterpart have also been unsuccessful (e.g., Leahy et al. 1992; Marti et al. 2000). However, 1E1740.7-2942 shows up prominently at radio wavelengths (Mirabel et al. 1992). In fact, the most remarkable property known of the source is the presence of persistent, two-sided radio jets, reminiscent of extragalactic radio-loud quasars. Such comparisons support the notion that 1E1740.7-2942 is an X-ray binary that contains an accreting black hole.

Shortly after its discovery, 1E1740.7-2942 generated a tremendous amount of excitement for being a possible source of electron-positron annihilation radiation (Bouchet et al. 1991; Sunyaev et al. 1991), which had been detected from the general direction of the Galactic center by earlier balloon-borne and space-borne experiments (see Harris 1997 for a historical account). Suggestions were subsequently made that the jets are perhaps made of electron-positron pairs ejected from the central black hole at relativistic speeds (Mirabel et al. 1992) and that the particles will eventually be slowed down and annihilated in the surrounding cold, dense molecular cloud. However, the reality of 1E1740.7-2942 being the “great annihilator” in the Galaxy has been brought into fierce debate, mostly because of the failure of detecting any annihilation features by the instruments aboard the *Compton Gamma-ray Observatory*, even in some of the simultaneous or contemporaneous observations with those of *SIGMA/GRANAT* on which the claims of detections were based (see review by Harris 1997). This remains a highly controversial issue.

To shed more light on the unusual environment surrounding 1E1740.7-2942, we observed the source with the *Chandra X-ray Observatory* (Chandra; Weisskopf & O’Dell 1997), taking advantage of the unprecedented spatial resolution that *Chandra* offers (van Spynbroeck et al. 1997). In this paper, we report the discovery of peculiar extended X-ray emission around 1E1740.7-2942, and present the first high-resolution X-ray spectra of the source.

2. Observation

1E1740.7-2942 was observed for about 10 ks on September 25, 1999 with the High-Energy Transmission Grating Spectrometer (HETGS; Canizares et al. 2000) on board *Chandra*, shortly after the Orbital Activation and Checkout phase of the mission. The grating spectra are read out by the spectroscopic array of the Advanced CCD Imaging Spectrometer (ACIS; Garmire et al. 2000) at the focal plane of the X-ray telescope. For the observation, we adopted an alternating exposure data mode with three primary (or long) frames (with a readout time of 3.3 s) followed by one secondary (or short) frame (with a readout time of 0.3 s). The reason for using the short frames is to obtain some zeroth-order data that is essentially free of the effects of “pile-up” (i.e., multiple photons hit the same event detection cell of the ACIS within one readout frame). This is important for observations of bright sources, such as 1E1740.7-2942, where serious pile-up is expected to distort the zeroth-order image. Although an unpile-up spectrum can be obtained from the higher-order grating data in this case, such data is of little use for imaging analysis. However, the use of alternating exposure modes reduces the observing efficiency. In our case, the effective exposure time is only about 6.7 ks and 0.2 ks for the long-frame data and short-frame data, respectively.

3. Data Analysis and Results

We received data products of the standard processing pipeline from the *Chandra* X-ray Center (CXC), in which the long-frame data and short-frame data were conveniently separated. We checked the (Level 2) products against all known caveats (listed at the CXC web site) for possible problems and found none (except for a known offset in the aspect solutions; see below). We then analyzed the Level 2 data with the *Chandra* Interactive Analysis of Observations software (version 1.1) which we obtained from the CXC. For some aspects of the spectral analysis we also used custom software as well as XSPEC version 10.0.

As expected, the global image (not shown) shows a compact X-ray emission region in the zeroth-order data and a characteristic “X” pattern of higher-order (or dispersed) spectra from two grating assemblies, the High Energy Grating (HEG) and Medium Energy Grating (MEG). The intrinsic energy resolution of the ACIS is relied upon for sorting out the overlapping orders of the dispersed spectra. In addition, a faint trace is visible in the long-frame image that runs through the zeroth-order image along the direction of frame transfer. This is an artifact resulting from photons hitting the CCD chip during the frame transfer operation. Therefore, such a “readout trace” is present only in the observations of bright X-ray sources. No other point sources were significantly detected over the entire field of view (roughly $8' \times 50'$).

3.1. Extended X-ray Emission

Zooming in on the zeroth-order image (shown in Fig. 1), we see that the innermost emission region appears to be elongated in the direction of northeast and southwest (but mostly east and west). In Fig. 1, we displayed an image made from the short-frame data and overlaid it with contours from the long-frame data. The image looks reasonably smooth and clearly shows a maximum at, presumably, the location of the point source. In contrast, the contours appear quite “lumpy” and actually show a local *minimum* at the source position. This is almost certainly due to the distortion of point spread function (PSF) caused by significant pile-up. The pile-up effects are obviously most severe at the position of the source and can cause an apparent “valley” there in the X-ray image. The effects can be crudely quantified by deriving the *expected* count rate of source in the zeroth-order image from that in the higher-order image, since the latter does not suffer from any pile-up. We determined that the expected zeroth-order count rate of the source should be about 1.9 count/s (or 6.3 count/frame), which explains the severe distortion of the PSF observed in the long-frame image. Actually, the situation is made worse by the fact that 1E1740.7-2942 has an unusually hard spectrum, which makes it more likely to cause additional “lost and undetected” events (Allen et al. 1998). Indeed, the measured count rate (from the zeroth-order image) is only about 0.03 count/s (compared to about 0.2 count/s for the extended emission surrounding the source). For the short-frame data, we estimated the count rate by adding up all the charge in the 3x3 event detection island around the central pixel in the 0th order image and determined a count rate of 1.28 count/s (or 0.38 count/frame), which corresponds to a $\sim 30\%$ pile-up (compared to the expected 1.9 count/s). For comparison, the measured count rate of the surrounding extended emission is about 0.3 count/s (which is significantly larger than that from the long-frame data, again indicating severe pile-up effects in that case). To quantify the effects of lost-and-undetected events for an unusually hard source like 1E1740.7-2942, we also ran PIMMs to estimate the pile-up rate. We obtained a significantly lower value, $\sim 20\%$, which can clearly be attributed to the fact that PIMMS does not take into account the lost-and-undetected events. Even at a pile-up rate of 30%, little distortion of the PSF is expected, based on the results from pre-flight ground calibration tests (Allen et al. 1998). However, the short-frame image suffers from the lack of statistics, due to the short exposure, which is why it does not show the faint “halo” emission (only about 0.04 count/s) surrounding the point source and the elongated feature (see outer contours in Fig. 1).

To quantify the elongation seen in the zeroth-order image, we ran MARX simulations (Wise et al. 1999) for the HETGS 0th order image of a point source which included the observed level of background. In Fig. 2., we fit the simulated MARX PSFs to the short-frame count profiles collapsed along the elongation and across it. The measured profile (solid line) across the elongation (top of Fig. 2) cannot be distinguished from a point source at a confidence level of 99.9%. Here we determined the full-width-at-half-maximum (FWHM) of the profile to be $0.83''$ (please note, the pointing of the observation was slightly off-axis to avoid the CCD node boundary). At roughly the same confidence level, we can exclude the possibility that the measured profile along the elongation is point-like. The width of the elongation is $1.35''$ FWHM.

Looking at Fig. 1 more carefully, the long-frame contours seem to indicate the presence of another region of extended emission, which lies to the south of the main feature. Given the severe distortion of the image by pile-up effects, however, it is entirely possible that this and the main feature are the integral part of the same extended emission. The smoothness of the short-frame image appears to support that. In addition, the fainter and more extended emission at the outer part of the image is statistically significant. It is approximately spherically symmetric about the point source and can be measured up to about $4''$ away from the source.

3.2. Position of 1E1740.7-2942

We derived the position of the point source in two ways. First, we constructed the zeroth-order count profiles along the right ascension (RA) and declination (Dec) from the the un-distorted short-frame image (in sky coordinates). We fitted the profiles with a simple Gaussian function to determine the position of the peaks. Although Gaussian functions are not a very good representation of the overall count profiles (especially around the wings), they are used only to fit a limited range around the peak of the profiles for determining the peak position. This allows us to measure the position to a sub-pixel accuracy, which is only limited by the signal-to-noise ratio (S/N) of the short-frame data.

Second, we utilized the fact that the point source should be at the intersection point of the readout trace and the dispersed MEG and HEG images. In this case, the problem of deriving the source position is over constrained, which allows a more realistic estimate of the uncertainties (including all systematic effects). We started by fitting a Gaussian function to the count profile across the readout trace (in the long-frame image) to determine its center. This gives the position of the source along one direction (nearly along the Dec) in sky coordinates. We then determined the position of the intersection point between the readout trace and the MEG or HEG images. The average of the two positions was used as the position of the source along the orthogonal direction (nearly along the RA). The difference between the them provides an estimate of the uncertainty in the source position derived using this technique.

For comparison, the results from both methods are summarized in Table 1. It is worth noting that the first method produced slightly smaller error bars, in spite of poorer statistics of the short-frame data. This can be understood in terms of systematic uncertainties in the dispersed HETGS traces and the faintness of the readout trace. We also note that there is a known offset ($\approx 2.09''$) in the aspect solutions for our observation (CXC web page). The numbers shown in the table have already been corrected for the offset. It is reassuring that the two methods are in an excellent agreement.

3.3. X-ray Spectra

We constructed the first-order (± 1) spectra of 1E1740.7-2942 from the MEG and HEG data. The higher-order data is ignored because of poor statistics. The individual spectra are compared for identifying common features which may only be marginal statistically in each case. The general agreement between the two MEG or HEG spectra or between the MEG and HEG spectra is good, although the statistics of the HEG data is poorer. To improve S/N, we first added the plus and minus orders for the MEG and HEG data separately; we then co-added the MEG and HEG first orders, with special care in deriving the wavelength scale for each spectrum. Fig. 3 shows the result. The spectrum was binned to $\sim 0.02 \text{ \AA}$ (which is about the energy resolution of the MEG). Note that there are hardly any counts above $\sim 5.5 \text{ \AA}$, because the source is known to be heavily absorbed. A crude fit to the continuum with a simple power law plus absorption yielded a hydrogen column density $11.8 \pm 0.6 \times 10^{22} \text{ cm}^{-2}$ and a photon index 0.90 ± 0.15 , in reasonable agreement with the ASCA results (Sheth et al. 1996; Churazov et al. 1996; Sakano et al. 1999). The integrated observed 2-10 keV flux is $2.2 \times 10^{-10} \text{ ergs s}^{-1} \text{ cm}^{-2}$. The flux error is of the order of 10%, which is the current status of calibration in the HETGS at high energies. The best-fit continuum model is also shown in Fig. 3 (in solid histograms) but is arbitrarily shifted down by 15% to accentuate possible line features (see below).

Deviations from the continuum model are quite apparent, mostly in the form of weak, narrow emission lines (though detected only at a significance level of roughly 2σ ; see Table 2). The feature at $\sim 1.74 \text{ \AA}$ (or $\sim 7.1 \text{ keV}$) appears to be an absorption edge, perhaps due to cold Fe atoms associated with the interstellar medium. The feature centered at $\sim 1.78 \text{ \AA}$ (or $\sim 6.96 \text{ keV}$) is probably due to the recombination line of H-like Fe ions (Fe XXVI). Note that the feature appears quite broad. Curiously, there appears to be two lines at 1.70 \AA and 1.96 \AA , respectively, which cannot be easily identified with any candidate elements. We speculate that these lines might also originate in the Fe XXVI recombination line but be blue- and red-shifted by the approaching and receding jets, respectively. It is worth pointing out that in this scenario the asymmetry of the lines about the rest-frame energy (see Fig. 3) would be expected because of the transverse Doppler shift. If the interpretation is correct, the observed radial and transverse Doppler shifts would imply that the velocity of the jets is about $0.26 c$ and the inclination angle (with respect to the line of sight) about 60° , assuming the approaching and receding jets are intrinsically identical. Applying the scenario to the remaining line candidates, we found that about 90% of them could be identified with H-like or He-like ions of Ca, S, and Ar and that the inferred blue- and red-shifted counterparts would give roughly the same jet parameters. Table 2 shows a list of the emission lines that are marginally detected, along with possible identifications, as well as the proposed Doppler-shifted counterparts of the lines. In contrast, we could only manage to identify about 40% of the lines without invoking any Doppler effects. Note that for the line candidates we only consider those that are present in at least three out of four first-order (± 1) MEG and HEG spectra. Any real spectral features in the HEG spectra should in principle always be present in the MEG spectra because of the improved statistics. The only exception is that a feature could fall right in the gap between two CCD chips

along the MEG arm of the “X” pattern.

The zeroth-order spectrum could, in principle, shed some light on the spectral properties of the extended emission. Unfortunately, severe pile-up causes significant distortion of the spectrum obtained from the long-frame data, while the short-frame data is not very useful due to its poor S/N. We could not tell with sufficient confidence whether there are any emission lines that are not present in the dispersed spectra (and thus would be associated with the extended emission). For comparison, when we binned the observed grating spectrum (Fig. 3) to the ACIS energy resolution (e.g., 0.05 Å at 1.85 Å), all features vanish, except for a merge between the ones at 1.71 Å and 1.78 Å. We chose not to pursue the subject any further in this work.

4. Discussion and Conclusions

For the first time, *Chandra* made it possible to image a possible black hole jet system, 1E1740.7-2942, with sub-arcsecond resolution in X-rays. Our primary motivation for conducting the observation was to search for X-ray emission from the jets themselves, both by direct imaging and by searching for Doppler-shifted emission lines as in the well-known case of SS 433 (Kotani et al. 1996).

We found no evidence for any jet emission in the X-ray image. Instead, we discovered a region (or regions) of extended emission. For comparison, a radio image of the system is shown in Fig. 4, with the inset showing an X-ray image of the region around the radio core that is overlaid by radio contours with comparable resolution. We can see that the main X-ray feature is elongated in the direction roughly orthogonal to the axis of the radio lobes. The extent of the elongation is about 3'', which corresponds to a linear size of ~ 0.12 pc, assuming that the distance to the source is 8.5 kpc. It seems, therefore, much too large to be associated with an accretion disk. We note that similar features have been detected in a recent VLBA+VLA observation of SS 433 (Paragi et al. 2000), although the extended radio emission is about a factor of 30 smaller than the main X-ray feature seen here in 1E1740.7-2942. It was speculated that the extended radio features in SS 433 might originate in the non-thermal radiation from relativistic electrons accelerated by shocks that are formed due to the interaction between the ejected matter from the accretion disk and the ambient medium (Paragi et al. 2000). Such an “excretion disk” scenario (through the L2 Lagrangian point) was thought to be possible for SS 433 during episodes of enhanced mass accretion. Perhaps, this scenario is also relevant for the much larger extended feature in 1E1740.7-2942. In this case, the extended X-ray emission observed could be due to the reprocessed radiation from the outflowing material that is illuminated by the central X-ray source. Alternatively, there might exist an equatorial wind from the companion star which produces the extended X-ray emission in a similar manner. In either case, fluorescent lines would be expected in the spectrum of the extended emission. Unfortunately, our data is not of sufficient quality to verify that.

On the other hand, it is perhaps worth asking whether the extended X-ray emission could

be associated with a previously unknown young supernova remnant (SNR). To see whether such a small SNR (of radius only 0.06 pc) is plausible, we adopt the Sedov-Taylor similarity solution (e.g., Osterbrock 1989):

$$R_s = 2t_{100}^{2/5} E_{51}^{1/5} N_0^{-1/5} \text{ pc}, \quad (1)$$

where R_s is the radius of the shock front, t_{100} is the time since the explosion in units of 100 years, E_{51} is the initial kinetic energy in units of 10^{51} erg, and N_0 is the number density of the ambient medium. Clearly, for any reasonable t_{100} and E_{51} , an enormous ambient density would be required to produce a SNR of the size of the observed extended X-ray feature. Besides, 1E1740.7+2942 and its vicinity has been observed with VLA, and no SNR has ever been detected (or reported). Therefore, we believe that the SNR scenario can be safely ruled out.

Although the identification of the radio counterpart of 1E1740.7-2942 is reasonably firm (Mirabel et al. 1993), there were always lingering doubts about the association of the X-ray source with the compact radio core. The sub-arcsecond spatial resolution of *Chandra* has now allowed us to measure the position of the X-ray source to an accuracy $\sim 0.06''$. The results (see Table 1) show that the X-ray source is about $0.6''$ east and $0.1''$ north of the compact radio core position. The difference between the X-ray and radio measurements is well within the uncertainty in the absolute astrometric solutions ($< 1''$; CXC web page). Given that in this case only one X-ray source is significantly detected over an approximately $8' \times 50'$ field of view, the probability of the source to fall, by chance, to within $\sim 0.6''$ of the radio core is $\sim 8 \times 10^{-7}$. It is worth emphasizing that such a bright source would have been detectable *anywhere* inside the field of view. Therefore, we conclude that it is highly unlikely that 1E1740.7-2942 was mis-identified at the radio wavelength.

The high-resolution HETGS spectrum of 1E1740.7-2942 shows evidence for emission lines (but only at roughly 2σ levels). The lines appear to be intrinsically narrow and weak, so they could have escaped the detections by previous X-ray spectrometers of inferior energy resolution (e.g., the GIS and SIS aboard ASCA; Sheth et al. 1996 and Churazov et al. 1996). The lines could be identified with H-like or He-like ions of Fe, Ca, S, and Ar. This would imply that the line-emitting material is highly ionized, which is perhaps not so surprising for an X-ray binary. The lines might originate from the accretion disk or the base of the jets where material moves relatively slowly. There is also evidence for the emission from the jets themselves, which is manifested in the pairs of Doppler red- and blue-shifted lines, although it is a bit speculative at present given the quality of the data. It is interesting to note, however, that every pair of lines would indicate approximately the same amount of Doppler shifts and that the inferred velocity and inclination angle of the twin jets are not unreasonable for this system (see § 3.3; compared to SS 433). A definitive confirmation or rejection of the proposed scenario awaits data of much improved S/N from future *Chandra* observations.

The faint, spherically symmetric halo emission is likely due to the scattering of X-rays from 1E1740.7-2942 by interstellar dust. Such scattering halos are known to exist around many X-ray sources and have proven useful for studying the spatial and size distributions of the dust grains in our Galaxy (e.g., Mauche & Gorenstein 1986; Predehl & Schmitt 1995). *Chandra* now makes it possible, for the first time, to directly image the phenomenon. The observations should, in

principle, allow us to derive spatially resolved energy distribution of photons in the halo and thus to test theoretical models at a more detailed level. Unfortunately, our observation does not provide sufficient statistics to warrant such an investigation.

We are grateful to Paul Plucinsky and his colleagues at CXC for clarifying several critical issues regarding the integrity of the pipeline products for our observation. We also thank Nancy Evans and her colleagues at the CXC help desk for providing a definitive answer to our inquiry regarding the uncertainty in the absolute aspect solutions. This work was supported in part by NASA through contract NAS8-38252. NSS and SCT wish to acknowledge support from NASA through the Smithsonian Astrophysical Observatory contract SAO SV1-61010, and IFM support from Conicet/Argentina.

REFERENCES

- Allen, C., et al. 1998, *SPIE*, 3444, 198
- Bally, J., & Leventhal, M. 1991, *Nature*, 353, 234
- Bouchet, L., et al. 1991, *ApJ*, 383, L45
- Churazov, E., Gilfanov, M., & Sunyaev, R. 1996, *ApJ*, 464, L71
- Cook, W. R., Grunsfeld, J. M., Heindl, W. A., Palmer, D. M., Prince, T. A., Schindler, S. M., & Stone, E. C., *ApJ*, 372, L75
- Harris, M. J. 1997, Proc. of the Fourth Compton Symposium, Eds. C. D. Dermer, M. S. Strickman, & J. D. Kurfess (New York: AIP), p. 418
- Hertz, P., & Grindlay, J. E. 1984, *ApJ*, 278, 137
- Kuznetsov, S., et al. 1997, *MNRAS*, 292, 651
- Leahy, D. A., Langill, P., & Kwok, S. 1992, *A&A*, 259, 209
- Lin, D., Smith, I. A., Bottcher, M. and Liang, E. P. 2000, *ApJ*, 531, 963
- Kotani, T., Kawai, N., Matsuoka, M., & Brinkmann, W. 1996, *PASJ*, 48, 619
- Marti, J., et al. 2000, in preparation
- Mauche, C. W., & Gorenstein, P. 1986, *ApJ*, 302, 371
- Mewe, R., Gronenschild, E. H. B. M., & van den Oord, G. H. J. 1985, *A&AS*, 62, 197
- Mirabel, I. F., Morris, M., Wink, J., Paul, J., & Cordier, B. 1991, *A&A*, 251, L43
- Mirabel, I. F., Rodríguez, L. F., Cordier, B., Paul, J., & Lebrun, F. 1992, *Nature*, 358, 215
- Mirabel, I. F., Rodríguez, L. F., Cordier, B., Paul, J., & Lebrun, F. 1993, *A&AS*, 97, 193
- Osterbrock, D. E. 1989, *Astrophysics of Gaseous Nebulae and Active Galactic Nuclei*, Mill Valley: University Science Books
- Paragi, Z., Vermeulen, R. C., Fejes, I., Schilizzi, R. T., Spencer, R. E., & Stirling, A. M. 2000, *A&A*, in press.
- Predehl, P., & Schmitt, J. H. M. M. 1995, *A&A*, 293, 889
- Phillips, J. A., Joseph, T., & Lazio, W. 1995, *ApJ*, 442, L37
- Sakano, M., Imanishi, K., Tsujimoto, M., Koyama, K., & Maeda, Y. 1999, *ApJ*, 520, 316
- Sheth, S., Liang, E., Luo, C., & Murakami, T. 1996, *ApJ*, 468, 755
- Skinner, G. K., et al. 1987, *Nature*, 330, 544
- Skinner, G. K., et al. 1991, *A&A*, 252, 172
- Smith, D. M., Heindl, W. A., Swank, J., Leventhal, M., Mirabel, I. F., & Rodríguez, L. F. 1997, *ApJ*, 489, L51

Sunyaev, R., et al. 1991, ApJ, 383, L49

van Speybroeck, L., Jerius, D., Edgar, R. J., Gaetz, T. J., Zhao, P., & Reid, P. B. 1997, Proc. SPIE, 3113, 98

Weisskopf, M. C., & O’Dell, S. L. 1997, Proc. SPIE, 3113, 2

Wise, M., et al. 1999, MARX 2.0 User’s Guide

Yan, M., & Dalgarno, A. 1997, ApJ, 481, 296

Table 1. Position of 1E1740.7-2942¹

Method	RA (J2000)	Dec (J2000)
1: PSF Fit	$17^h 43^m 54^s.876 \pm 0.004$	$-29^\circ 44' 42''.48 \pm 0.04$
2: HETG Fit	$17^h 43^m 54^s.878 \pm 0.005$	$-29^\circ 44' 42''.53 \pm 0.09$
Radio Position ²	$17^h 43^m 54^s.83$	$-29^\circ 44' 42''.60$

¹The uncertainties shown represent roughly 90% confidence limits, except for those on the RA from the second method (see text).

²The radio coordinates were derived from an expanded dataset, as shown in Fig. 4, and the position is slightly different from those given by Mirabel et al. (1992).

Table 2. Possible Emission Lines from 1E1740.7-2942¹

Ion Name	Rest-Frame λ (Å) ²	Measured λ (Å) ³	Blue-Shifted λ (Å) ³	Red-Shifted λ (Å) ³
Fe XXVI	1.78	1.78	1.70	1.96
Ca XX	2.24	2.24	2.14	2.42
	2.54	2.54	2.44	2.68
	3.04	3.04	2.93	... ⁴
Ca XIX	2.60	2.60
	3.21	3.21	3.11	3.42
S XVI	3.65	3.64	3.54	3.81
	4.73	4.71	4.61	4.90
Ar XVII	3.95	3.95	3.86	4.14
S XV	4.31	4.31	4.21	4.54
	5.04	5.04
Si XVI	4.95	4.95

¹All lines were detected only at a significance level of roughly 2σ . The equivalent width is typically $\lesssim 0.3\%$ of the wavelength of a line.

²From Mewe et al. (1985).

³The measurement accuracy is about 0.02 \AA , corresponding to the size of the MEG data bins.

⁴The line seems to be blended with those of Ca XIX.

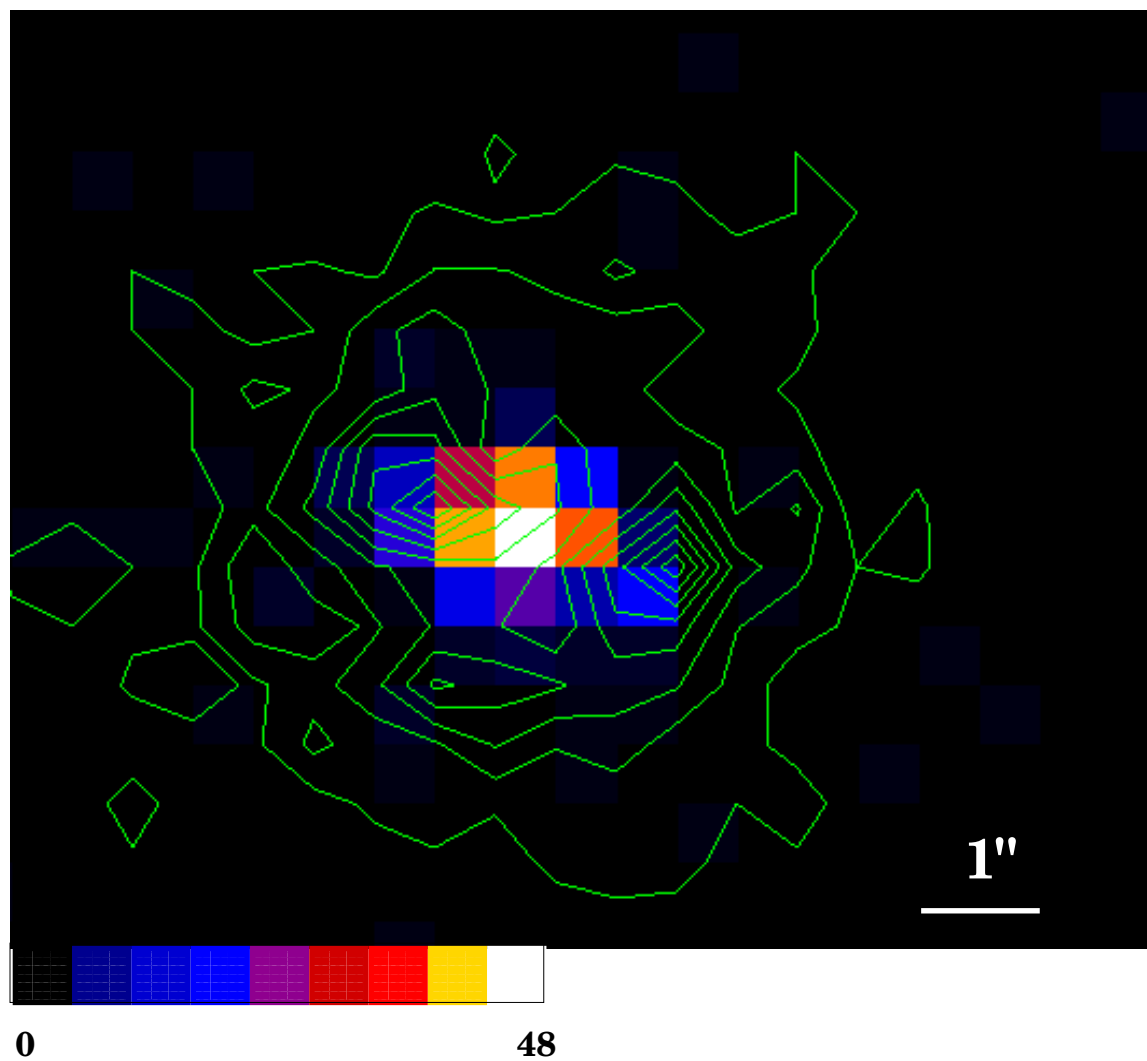


Fig. 1.— Unsmoothed X-ray image of 1E1740.7-2942. The image is made from the short-frame data (with pixel size $0.492''$) and the overlaying contours are from the long-frame data. The image is color coded linearly based on the observed X-ray intensity (in terms of total counts). The color scheme is shown at the bottom. The contours are in the range of 5 to 43 counts, with a linear step size of 4.75 counts. Note the “lumpiness” of the contours is an indication of significant pile-up in the long-frame data.

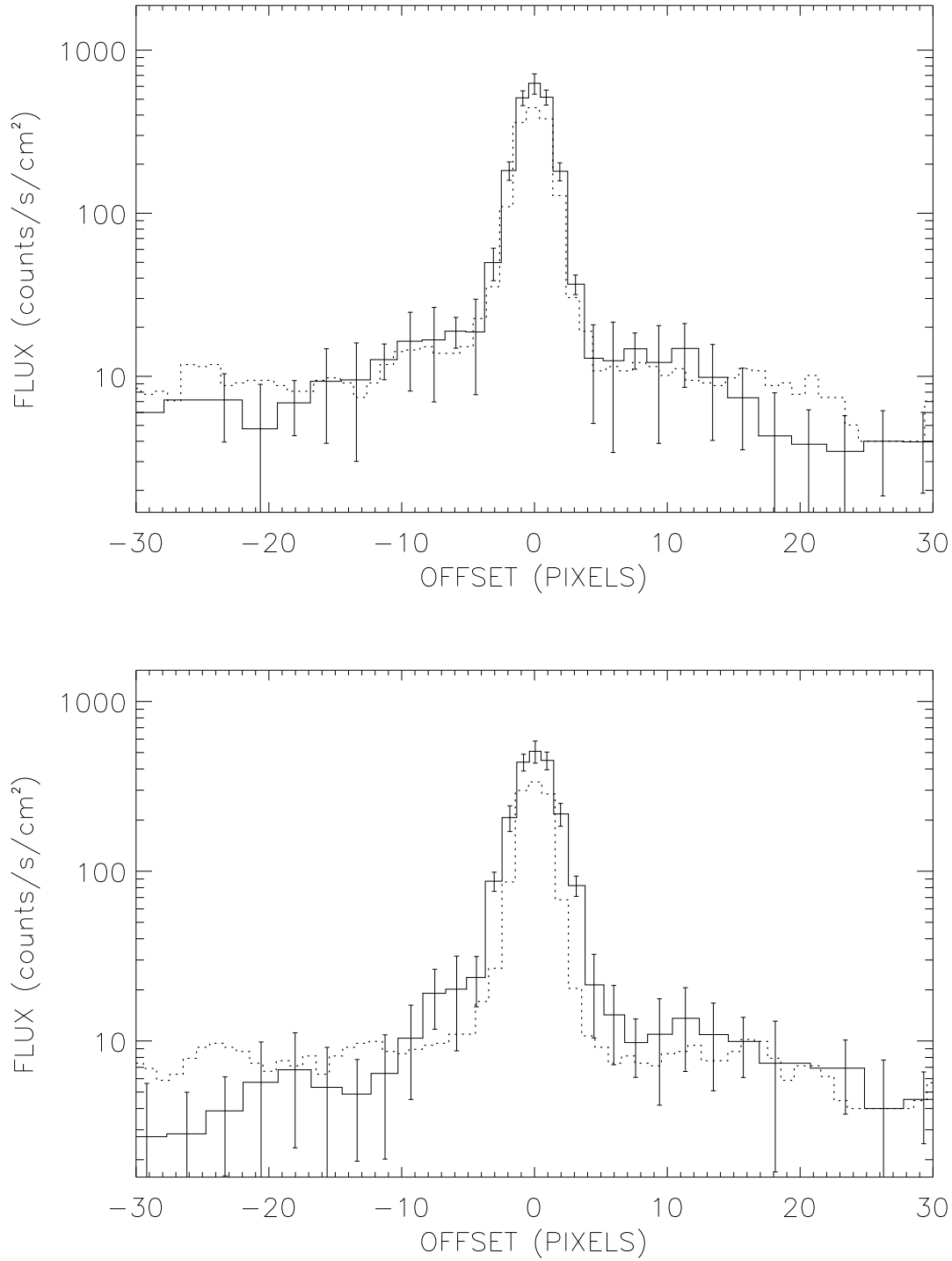


Fig. 2.— Linear profiles of the extended emission (in solid histograms). The profiles were made by collapsing the observed counts along the direction of the elongation (bottom) and across it (top), respectively. The best-fit MARX simulated point-spread functions (PSFs) are also shown in dashed histograms.

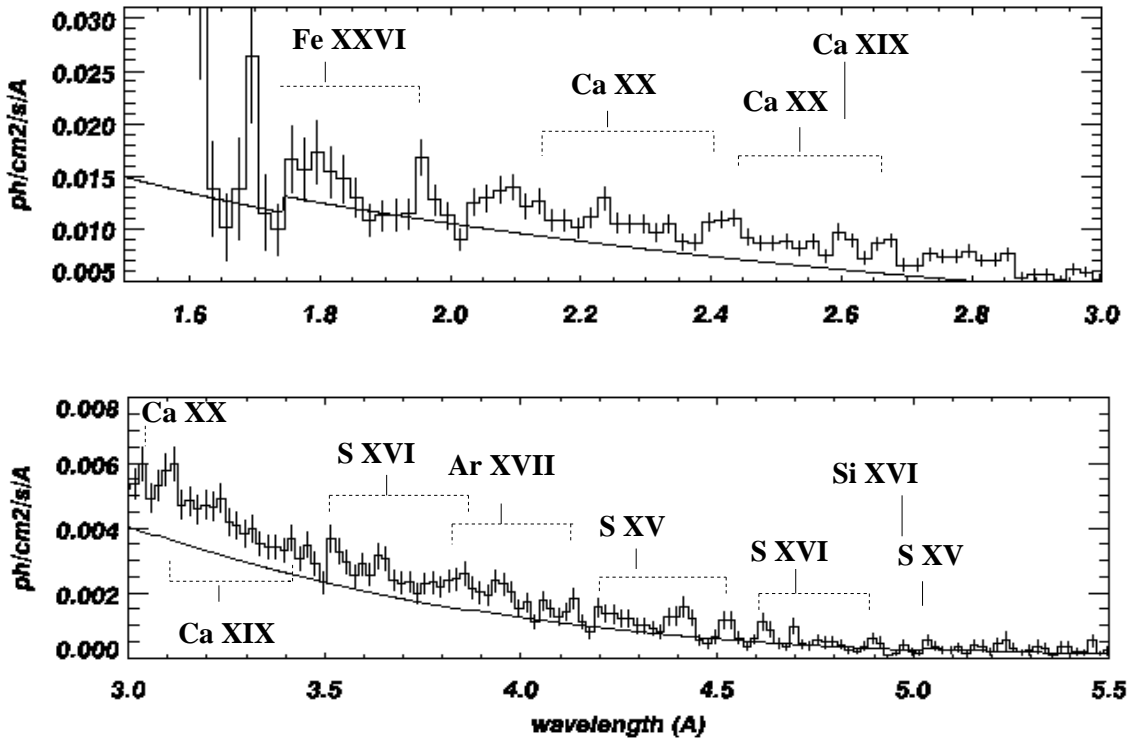


Fig. 3.— The first-order MEG spectrum of 1E1740.7-2942. The data is binned to 0.02 \AA , which is roughly the MEG resolution. The best-fit continuum model is also shown in solid line but is arbitrarily shifted down by 15% to highlight possible emission lines. Each line candidate, as well as its proposed Doppler-shifted pairs, is marked with a tentative identification (see text).

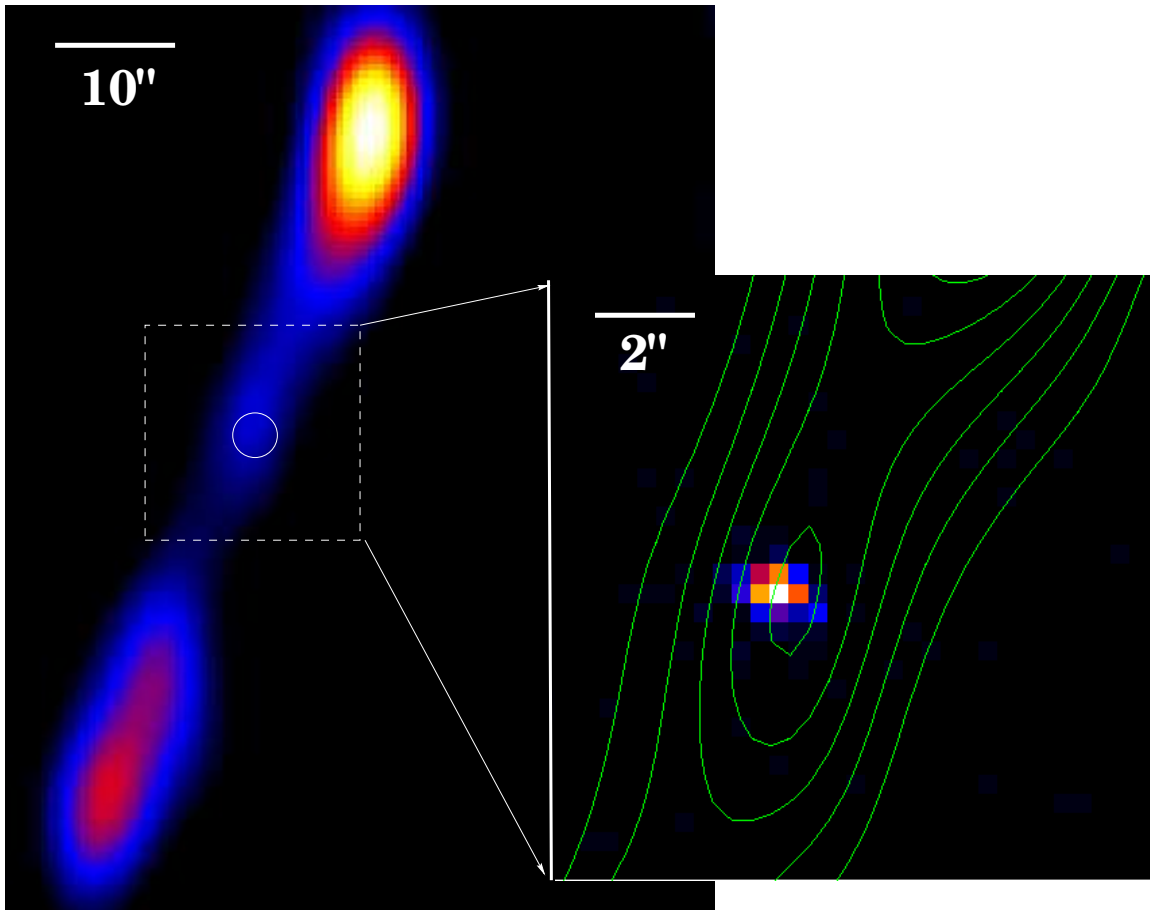


Fig. 4.— Comparison of X-ray and VLA radio (6-cm) images of 1E1740.7-2942. The main panel shows the compact radio core and extended lobes (or jets) and the inset shows the short-frame image overlaid by the radio contours for a smaller central region (as indicated in the main panel). The small circle in the main panel is indicative of the spatial extent of the X-ray emission observed. Note a small residual discrepancy between the position of the X-ray source and that of its radio counterpart.